Structural and magnetic properties of orthorhombic Li$_x$MnO$_2$

D.G. Kellerman [a,*], J.E. Medvedeva [b], V.S. Gorshkov [a], A.I. Kurbakov [c,d],
V.G. Zubkov [a], A.P. Tyutyunnik [a], V.A. Trunov [c]

[a] *Institute of Solid State Chemistry, Ural Division, Russian Academy of Sciences, Pervomaiskaya 91, GSP-145, 620041 Ekaterinburg, Russia*
[b] *Department of Physics, University of Missouri, Rolla, MO 65409, USA*
[c] *Konstantinov St. Petersburg Nuclear Physics Institute, Russian Academy of Sciences, Gatchina, Leningrad Oblast 188300, Russia*
[d] *Laboratory Léon Brillouin, CE Saclay, 91191 Gif-sur-Yvette, France*

Abstract

Rietveld refinement of the crystal and magnetic structures of Li$_x$MnO$_2$ ($x = 0.98$, 1.00, 1.02) are performed using neutron and X-ray measurements. A significant structural disorder due to the presence of manganese ions in lithium positions (Mn$_{Li}$) and lithium ions in manganese ones (Li$_{Mn}$) is found to be a common feature of Li$_{0.98}$MnO$_2$, Li$_{1.00}$MnO$_2$, and Li$_{1.02}$MnO$_2$.

An essential anisotropy of the thermal-expansion coefficients of the lithium manganese oxides is observed in the temperature range of 1.5−300 K. Furthermore, the distortion of the oxygen octahedral environment around the manganese ions decreases when the temperature lowers. This is attributed to the strong exchange interactions between parallel exchange-coupled Mn chains. First-principles calculations of the effective exchange-interaction parameters in Li$_{16}$Mn$_{16}$O$_{32}$ confirm the essential antiferromagnetic interactions between the chains. In addition, a hypothetical (Li$_{15}$Mn)Mn$_{16}$O$_{32}$ structure where a lithium atom located between the Mn double layers is replaced by a manganese atom is considered. The calculations reveal that the presence of such defects results in appearance of a ferromagnetic component that agrees with the magnetic measurements.
© 2006 Elsevier Masson SAS. All rights reserved.

Keywords: Lithium manganese oxide; Magnetic susceptibility; Neutron diffraction; X-ray diffraction; Exchange parameter; First-principles calculation

1. Introduction

The attempts to create a high-effective cathode material for Li-ion batteries draw an increased attention to the Li−Mn−O systems. Lithium manganese oxide, LiMnO$_2$, is considered as a possible alternative to well-known lithium manganese spinel, LiMn$_2$O$_4$, due to a larger theoretical capacity of the former [1,2]. However, to date, high characteristics of LiMnO$_2$ have not been reached − despite numerous attempts to employ new techniques of synthesis [3−5]. One of the reasons that prevent to achieve the required cathode characteristics in LiMnO$_2$ is the structural peculiarities of this material. Hence,

detailed structural investigations of lithium manganese oxides with various defects are of great interest.

The orthorhombic structure of LiMnO$_2$ (*Pmmn*) [6] (Fig. 1) is one of the variants of the ordered rock-salt cubic structure. Strong magnetic interactions between Mn^{3+} ions and the Jahn−Teller effect are considered [7] as possible reasons for the stabilization of an orthorhombic structure. These very factors play an important role in magnetic behavior of LiMnO$_2$ as well. Studies of the magnetic properties of both stoichiometric LiMnO$_2$ and that with structural defects are useful because of not only the non-trivial nature of the magnetic interactions but also the possibility to predict the material behavior in the electrochemical cell.

The first data on the magnetic properties of the orthorhombic LiMnO$_2$ can be found in Bongers' report [8], where an antiferromagnetic transition at 300 K was observed. The results

* Corresponding author. Tel.: +7 343 3623442.
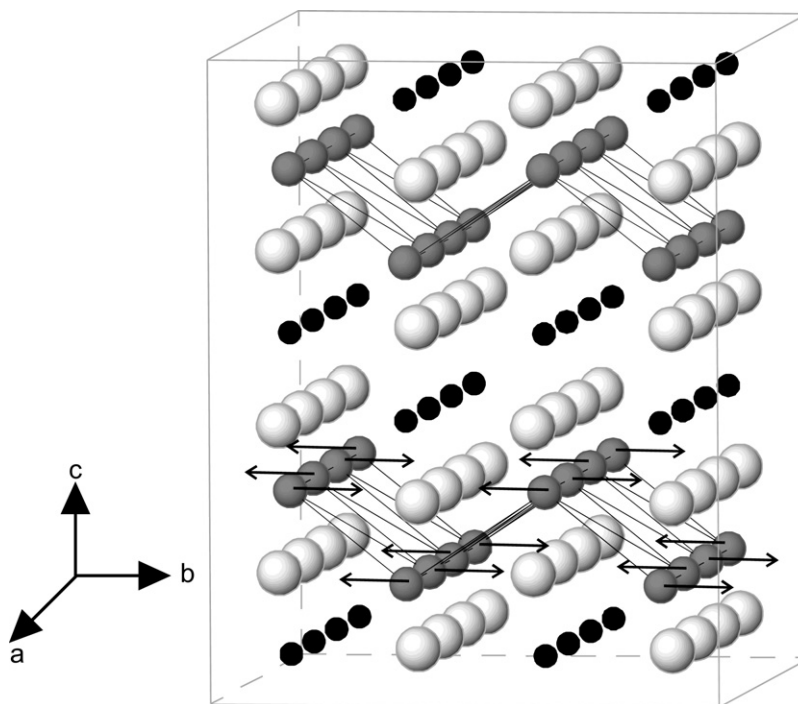*E-mail address:* kellerman@ihim.uran.ru (D.G. Kellerman).

Fig. 1. Fragment of $LiMnO_2$ crystal structure. ● − Li, ● − Mn, ○ − O. Arrows indicate magnetic moment directions in antiferromagnetic phase.

were later confirmed by more detailed investigations [9−11]. The main features of magnetic susceptibility are the following: the paramagnetic behavior follows the Curie−Weiss law at the temperature above 600 K ($\Theta = -949$ K, $\mu_{eff} = 4.79\ \mu_B/Mn^{3+}$ [10]); a broad maximum of susceptibility polytherms at 360 K and field cooled (fc) and zero field cooled (zfc) divergence below 100 K. The magnetic structure of $LiMnO_2$ with a propagation vector, $k = (1/2\ 1/2\ 1/2)$, and magnetic moment 3.69 μ_B/Mn^{3+} with a preferred direction along the b-axis has been proposed on the basis of neutron-diffraction data [9]. The Néel temperature, T_N, characterizing transition to the phase with three-dimensional order, is 261.5 K [9]. Short-range order effects are observed above this temperature. As shown in Ref. [10], at $T > 300$ K the magnetic properties of $LiMnO_2$ are well described by a model of exchange-bound chains with an exchange-interaction parameter, $J = -36.5$ cm^{-1}. At $T < 50$ K, magnetic behavior which may be related to weak ferromagnetism, has been observed [9,11].

Here, we employ both experimental and theoretical approaches to study the role of defects in the structural and magnetic properties of lithium manganese oxide Li_xMnO_2.

2. Experiment

2.1. Materials

In order to investigate the role of structural defects in the properties of lithium manganese oxides Li_xMnO_2 samples with deficit and excess of lithium were synthesized. Lithium content in starting mixture was $0.94 < x < 1.06$. The synthesis has been performed by mixing Mn_2O_3 and Li_2CO_3 in

calculated proportions, grinding and annealing at 750 °C under helium atmosphere for 25 h. The phase composition of the samples was checked by X-ray powder diffraction (XRD). In the region $0.97 < x < 1.02$, only orthorhombic phase was revealed. At lower lithium concentration traces of spinel phase were detected. The samples with $x \geq 1.03$ contained Li_2MnO_3 traces. So the $Li_{0.97}MnO_2$, $Li_{1.00}MnO_2$, and $Li_{1.02}MnO_2$ compositions were selected to study. Lithium and manganese contents were analyzed using atomic absorption analysis on samples dissolved in 2.5 M hydrochloric acid. The observed Li/Mn ratios are practically the same as the nominal ones (0.98, 1.00 and 1.02, correspondingly). To determine the average manganese oxidation state permanganate back-titration of the reduced samples was performed. It was demonstrated that manganese oxidation state is the same in all samples under consideration and does not differ from that in stoichiometric 'LiMnO$_2$'.

2.2. Methods

Neutron powder diffraction data were collected in the temperature region of 1.5−290 K with a G4.2 neutron powder diffractometer (ORPHEE reactor, Saclay, France; $\lambda_0 = 2.343$ Å; $3 < 2\theta < 174°$, 0.1° step, $\Delta d/d_{min} = 0.2\%$). All the XRD patterns were collected on a transmission STADI-P (STOE, Germany) diffractometer equipped with a scintillation detector, using Cu Kα_1 radiation in the 2θ range 2°−120° with a step of 0.02°. Polycrystalline silicon ($a = 5.43075(5)$ Å) was used as external standard. The ''Base of JCPDS-ICDD PDF2 powder standards'' (ICDD, USA, version 2005) was used for identification of possible impurity phases. The crystal structure of the

samples studied was refined by a GSAS program [12] using both neutron and X-ray data. Line profile was approximated by the pseudo-Voigt function: $I(2\Theta) = \eta L(2\Theta) + (1 - \eta)G(2\Theta)$, where L and G are the Lorentz and Gauss functions, respectively; and the angular line-width of a line was done by the relationship: $(FWHM)^2 = Utg^2\Theta + Vtg\Theta + W$, where FWHM is a full line width on the half maximum. Background level was specified as a combination of 15 Chebyshev polynomials.

Magnetic susceptibility in the temperature range of 1.5–300 K was measured by a MPMS-5XL (Quantum Design) SQUID-magnetometer in the fields up to 50 kOe, while at 77–1000 K, it was done by the Faraday method in fields up to 10 kOe.

2.3. Theoretical methods

First-principles electronic structure investigations were performed within a linearized muffin-tin orbitals method [13] in the atomic-spheres approximation (LMTO-ASA). The effective exchange-interaction parameters were calculated as the second derivative of total energy of the ground state with respect to the angle of the magnetic-moment rotation [14]. To determine the exchange-interaction parameters between the nearest manganese atoms (or next nearest ones) that belong to (1) the same structural layer, (2) two closest structural layers in a double layer, or (3) different double layers, a supercell containing 16 formula units of $LiMnO_2$ was used. In addition, 64 empty spheres were introduced into the system because the structure is not close-packed.

3. Results and discussion

3.1. Refinement of the crystal structure of $Li_{0.98}MnO_2$, $Li_{1.00}MnO_2$, and $Li_{1.02}MnO_2$

Structural data refined for three compositions of Li_xMnO_2 are shown in Tables 1 and 2. (Standard deviations are given in brackets; r and n indices stand for the X-ray and neutron data, respectively.) These results are in good agreement with those obtained previously in Ref. [6].

Based on the small differences in the chemical composition of the samples under consideration, one can argue that the structural parameters should not vary essentially. However, the detailed analysis of data given in Tables 1 and 2, reveal some important tendencies. First, we note that the size of the unit cell of Li_xMnO_2 increases with lithium concentration. Lattice expansion is observed in all directions and may

Table 1
Orthorhombic unit cell parameters of $Li_{0.98}MnO_2$, $Li_{1.00}MnO_2$ and $Li_{1.02}MnO_2$

Parameter	$Li_{0.98}MnO_2$	$Li_{1.00}MnO_2$	$Li_{1.02}MnO_2$
a (Å)	2.80473(4)	2.80644 (3)	2.80661(2)
B (Å)	4.57419(8)	4.57536(7)	4.57749(4)
c (Å)	5.74873(9)	5.75092(8)	5.75147(5)
V (Å³)	73.753(2)	73.845(2)	73.891(1)

Table 2
Structural and isotropic thermal (U_{iso} (Å²)) parameters for $Li_{0.98}MnO_2$, $Li_{1.00}MnO_2$ and $Li_{1.02}MnO_2$ (s.g. Pmnm)

			$Li_{0.98}MnO_2$	$Li_{1.00}MnO_2$	$Li_{1.02}MnO_2$
2a	x/a		1/4	1/4	1/4
	y/b		1/4	1/4	1/4
	z/c		0.114 (2)	0.114(1)	0.115 (2)
	$U_{iso} \times 100$		2.4(1)	2.5(1)	2.1(1)
	Occupancy	Li	0.972(2)	0.980(2)	0.990(2)
		Mn	0.028(2)	0.020(2)	0.010(2)
2a	x/a		1/4	1/4	1/4
	y/b		1/4	1/4	1/4
	z/c		0.6336(4)	0.6345(3)	0.6348(3)
	$U_{iso} \times 100$		1.24(5)	1.28(4)	1.24(4)
	Occupancy	Mn	0.995(6)	0.984(5)	0.974(5)
		Li	0.005(6)	0.016(5)	0.026(5)
2b	x/a		1/4	1/4	1/4
	y/b		3/4	3/4	3/4
	z/c		0.1414(6)	0.1418(5)	0.1415(6)
	$U_{iso} \times 100$		2.08(6)	1.79(5)	1.55(5)
	Occupancy	O1	1.00	1.00	1.00
2b	x/a		1/4	1/4	1/4
	y/b		3/4	3/4	3/4
	z/c		0.6006(6)	0.6011(5)	0.6010(5)
	$U_{iso} \times 100$		1.81(6)	1.65(5)	1.70(5)
	Occupancy	O2	1.00	1.00	1.00
Agreement factors	$\omega R_p(r)$		5.25	4.03	4.53
	$\omega R_p(n)$		5.80	5.07	5.50
	$R_p(r)$		3.25	2.61	2.77
	$R_p(n)$		4.33	3.77	3.82
	$\chi^2(r)$		2.565	1.639	1.982
	$R(F^2)(r)$		5.94	6.28	6.27
	$R(F^2)(n)$		6.43	4.05	3.12

ωR_p – weighted profile factor; R_p – profile factor; χ^2 – goodness of fit; $R(F^2)$ – Bragg factor; r and n denote X-ray and neutron data, respectively.

be attributed to the difference between the ionic radii of manganese and lithium.

A common feature of $Li_{0.98}MnO_2$, $Li_{1.00}MnO_2$ and $Li_{1.02}MnO_2$, detected during full-profile analysis of X-ray and neutron data, is a structural disorder caused by the presence of manganese ions in lithium positions (Mn_{Li}) and lithium ions in manganese ones (Li_{Mn}). Previously the cationic disorder in $LiMnO_2$ was assumed both from the analysis of the ESR-spectra [11], and from X-ray diffraction study [15].

The results of the calculations suggest that both LiO_6 and MnO_6 octahedra are strongly distorted as well and are elongated along the b-axes. The tetragonal distortion observed for the oxygen octahedra, which is found to be around 19% at room temperature, is due to the Jahn–Teller effect. The type of tetragonal distortion in $LiMnO_2$ suggests that the $Mn^{3+}(3d^4)$ has the electron configuration $t_{2g}^3 d_{z^2}^1 d_{x^2-y^2}^0$.

The parameters of the orthorhombic cell of $LiMnO_2$ are related to a hypothetical parent cubic lattice parameter (a') by the following formulae: $a = 1/2\sqrt{2}a'$, $b = a'$, and $c = \sqrt{2}a'$ (*) [16], it follows that $b/a \approx 1.41$, $b/c \approx 0.707$, and $c/a = 2$. However, the experimental structural ratios (Table 3) suggest that the b-parameter of the orthorhombic lattice is considerably larger than the theoretically predicted one using (*). Thus, we can conclude that in the case of $LiMnO_2$, notable "tetragonal" distortions of the structure exist, and Jahn–Teller effect has

Table 3
Lattice parameters ratios for $Li_{0.98}MnO_2$, $Li_{1.00}MnO_2$ and $Li_{1.02}MnO_2$ at 300 and 1.5 K

Compound	300 K			1.5 K		
	b/a	b/c	c/a	b/a	b/c	c/a
$Li_{0.98}MnO_2$	1.631	0. 796	2.049	1.616	0.788	2.050
$Li_{1.00}MnO_2$	1.630	0.796	2.048	1.617	0.789	2.049
$Li_{1.02}MnO_2$	1.631	0.796	2.049	1.618	0.790	2.048

a cooperative character. This is pointed out by the correlation between the changes in the unit cell parameters and the distortions of the local oxygen neighbors of the manganese ions, in particular, when the temperature decreases (Table 3, Fig. 2c).

Let us follow the changes in the structural parameters of $Li_{0.98}MnO_2$, $Li_{1.00}MnO_2$, and $Li_{1.02}MnO_2$ when the temperature decreases from 300 to 1.5 K. Analysis of neutron-diffraction data shows that the lattice compression occurs along each of the three directions in this temperature range. However, whereas the relative change of the a and c parameters for each composition does not exceed 0.1%, the compression of the orthorhombic lattice along the b-axis is one order of magnitude larger than along the other two directions

(Fig. 2a,b). Besides that when the temperature decreases, the local environment of lithium and manganese atoms changes due to a decrease of the degree of distortion of the oxygen octahedra (Fig. 2c). Anisotropy of the thermal-expansion coefficients of lithium manganese oxide can also be demonstrated based on the relative change of the unit cell parameters (Table 3). Reduction of the b/c and b/a ratios points to a decrease of the tetragonal distortions at lower temperatures.

Usually, a stable macroscopic distortion of a crystal caused by the Jahn−Teller effect is observed at rather low temperatures [17]. As the temperature increases, an entropy term prevails over the interaction related to the cooperative distortion of the lattice and this tends eventually to suppress the macroscopic deformation. In this sense, the observed behavior of $LiMnO_2$ is non-trivial because the deformation lowers not when the temperature increases but when it decreases. The observed reduction of the oxygen octahedra distortion in $Li_{0.98}MnO_2$, $Li_{1.00}MnO_2$, and $Li_{1.02}MnO_2$ (Fig. 2), testifies that there are some additional competitive interactions in the system which are responsible for the compression of the octahedra as the temperature decreases. Since the octahedra are extended along the b-axis of the orthorhombic structure of
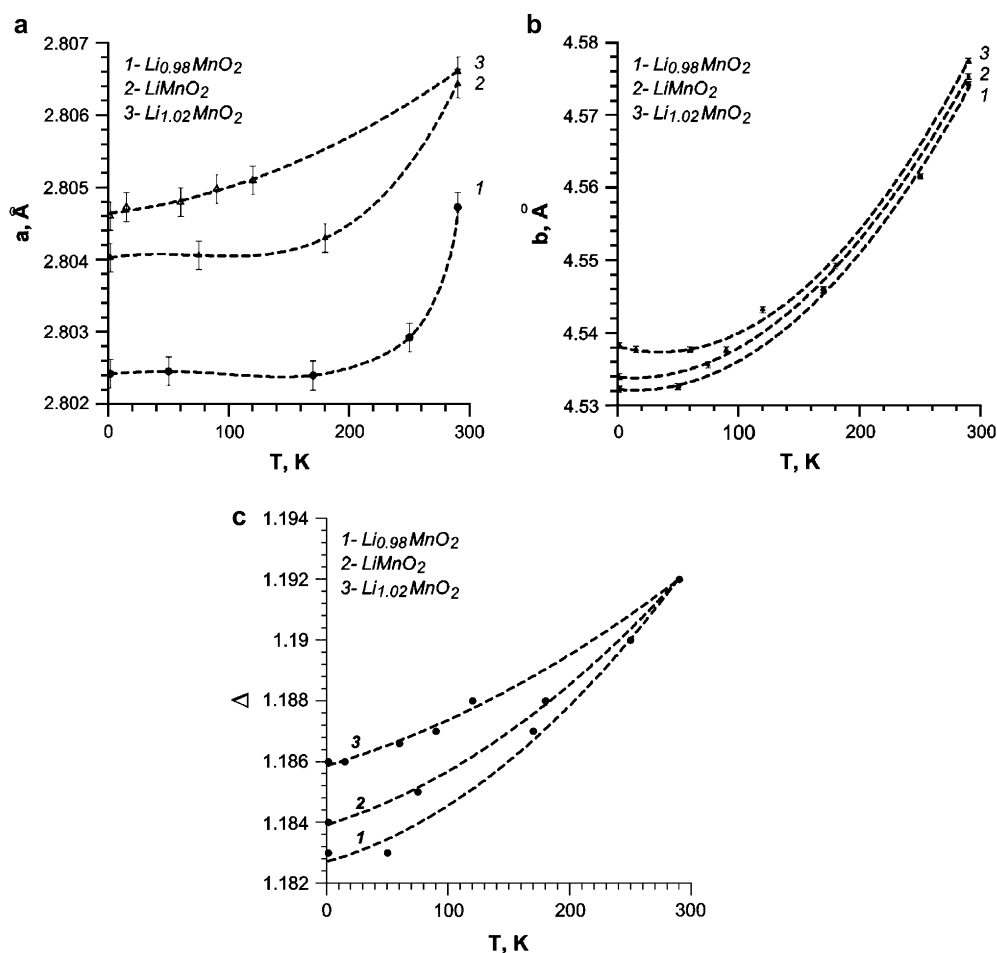

Fig. 2. Variations of a and b unit cell parameters and tetragonal distortion of MnO_6 octahedron ($\Delta = 2r_b/(r_a + r_c)$) with temperature in $Li_{0.98}MnO_2$, $Li_{1.00}MnO_2$, and $Li_{1.02}MnO_2$.

lithium manganese oxide, the interactions that counteract such deformation should be along the same axis. In our opinion, the exchange interactions between manganese ions can play an important role. As considered earlier in Ref. [10], the magnetic properties of $LiMnO_2$ are well described by a model of parallel exchange-coupled chains of Mn atoms. The chains are arranged along the a-axis (Fig. 1). The half-filled d_{z^2} orbitals elongated in the direction perpendicular to the chain are involved in the exchange between the chains, namely in the indirect 180° exchange through the oxygen ion located between two manganese ions (Fig. 3).

The phenomenon that leads to reduction of the degree of the oxygen-octahedron distortion and to anisotropic compression of lithium manganese oxide lattice may be considered as a magnetostriction effect: the total energy of the crystal decreases due to the magnetocrystal energy changes caused by stress and hence the changes in the exchange-interaction energy [18]. Using CoO as an example, Kanamori has considered the exchange interactions as possible origin of the striction effects [19].

3.2. First-principles calculations of the exchange-interaction parameters in $Li_{16}Mn_{16}O_{32}$

In order to show that the interchains exchange interactions are important and may cause striction effects, we calculated the main exchange-interaction parameters in the orthorhombic structure of $LiMnO_2$ as shown in Fig. 4. The results are summarized in Table 4. To determine the exchange-interaction parameters between the nearest manganese atoms (or next nearest ones) that belong to (1) the same structural layer, (2) two closest structural layers in a double layer, or (3) different double layers, a supercell containing 16 formula units of $LiMnO_2$, was used in calculations to make it possible to determine the values of exchange interactions between the nearest manganese atoms (or next nearest ones) being among (1) a structure layer, (2) various structure layers, and (3) different double layers. Thus the total number of atoms in a supercell is 64. Furthermore, in addition, 64 empty spheres were introduced into the system because this structure was not close-packed. First of all, we found a strong anisotropy of the exchange interaction — in agreement with our experimental results mentioned above: according to the peculiarities of the crystal structure of $LiMnO_2$, the largest exchange-interaction parameter is obtained for the linear chains along the a-axis.

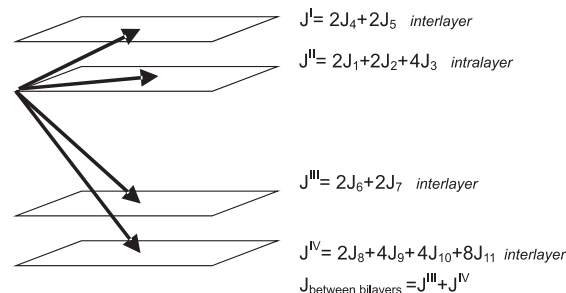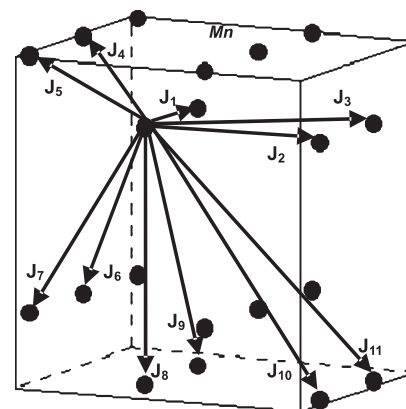Fig. 3. Schematic representation of the 180° interchain exchange coupling in $LiMnO_2$.

Fig. 4. Exchange interactions in ideal $LiMnO_2$.

This interaction is antiferromagnetic with $J_1 = -86.28$ meV. We note, however, that antiferromagnetic interaction between Mn chains is also strong, $J_2 = -62.41$ meV. Further, the calculated exchange-interaction parameters between the Mn^{3+} ions which belong to a double layer, J_4 and J_5, are three times smaller than those along the chains, while the exchange interactions between double layers are negligible. The total parameter characterizing the interaction in a layer is one order of magnitude larger than the one corresponding to the interaction between double layers (Table 4).

Table 4
Calculated exchange parameters for $Li_{16}Mn_{16}O_{32}$ and $(Li_{15}Mn)Mn_{16}O_{32}$

J (meV)	$Li_{16}Mn_{16}O_{32}$	$(Li_{15}Mn)Mn_{16}O_{32}$
J_1	−86.28	−77.03
J_2	−62.41	−52.26
J_3	+1.60	+2.04
J_4	−21.15	−15.36
J_5	−17.03	−8.91
J_6	−0.52	−0.39
J_7	−0.37	+2.12
J_8	−0.87	−0.05
J_9	+0.008	+0.39
J_{10}	−0.02	+0.19
J_{11}	+0.00	+0.12
J^I	−76.36	−48.54
J^{II}	−290.98	−262.50
J^{III}	−1.78	+3.46
J^{IV}	−1.5	+3.18
$J_{between\ bilayers}$	−3.28	+6.64
J_{defect}	–	−49.71

Thus, first-principles calculations show that the exchange interaction between manganese ions, which belong to the parallel chains along the a-axis, is large and may be responsible for striction effects leading to the lessening of the octahedra deformation when the temperature decreases.

3.3. $Li_{1-x}Mn_xO_2$ magnetic structure and properties

As shown in Refs. [9] and [10], the magnetic susceptibility of $LiMnO_2$ has a number of peculiarities. First, a broad maximum is observed near 360 K. This temperature is essentially higher than the Néel temperature. The maximum has been attributed to the presence of the exchange-coupled clusters, and infinite chains along the a-axis have been considered as such clusters [10]. At the temperature of maximum the thermal energy becomes comparable to the energy of the exchange interactions, so the magnetic chains break down transforming gradually into an ensemble of single paramagnetic centers. As seen from Fig. 5, chains with smaller concentration of Li_{Mn}-defects are maintained up to a higher temperature: 358, 366, and 380 K for $Li_{1.02}MnO_2$ $Li_{1.00}MnO_2$, and $Li_{0.98}MnO_2$, respectively. Thus, the existence of the over-stoichiometry lithium in Li_xMnO_2 results in weakening of the two-dimensional interactions.

Additional reflections attributed to the magnetic-ordering process were detected on the neutron-diffraction powder patterns of all considered samples at $T < T_N$. There is a regular increase of the intensity of the magnetic reflections as the temperature decreases. Rietveld refinement of the nuclear and magnetic components of the spectra using a GSAS program complex, shows that main characteristics of the magnetic structure are independent of the lithium/manganese relation and coincide with the results [9] obtained for the stoichiometric

$LiMnO_2$. Our calculations demonstrate that for all compositions, the magnetic unit cell is characterized by the doubled parameters in all three directions: $2a \times 2b \times 2c$. The results of the refinement of the magnetic structure of $Li_{0.98}MnO_2$, $Li_{1.00}MnO_2$, and $Li_{1.02}MnO_2$ at 1.5 K are given in Table 5.

The magnetic structure of $LiMnO_2$ consists of antiferromagnetically ordered chains along the a-axis. The interaction between the chains located in the same plane is antiferromagnetic as well. Antiferromagnetic interaction also binds (i) the chains located within a corrugation layer and (ii) the neighboring chains. Furthermore, all magnetic moments are ordered along the b-axis of the orthorhombic structure of $LiMnO_2$ (Fig. 1). We note here, that the results of the refinement of the magnetic structure agree with the results of the first-principles calculations that show that the main interactions in lithium manganese oxide have an antiferromagnetic character.

An increase of the lithium concentration in Li_xMnO_2 favors some changes of the magnetic cell constants (Table 5). Besides, certain changes are found in the value of the magnetic moment that corresponds to the manganese ion. This is clearly seen from both the data given in Table 5 and the temperature dependence of the magnetic moment (Fig. 6). A decrease of the magnetic moment when the temperature increases is quite a usual behavior that reflects disappearance of the magnetic order. However, while the variations in the values of the magnetic moment for $Li_{0.98}MnO_2$ and $Li_{1.00}MnO_2$ are within the error limits, the μ_{Mn} for $Li_{1.02}MnO_2$ is much lower (around 8%). The lower magnetic moments for the composition with higher concentrations of lithium may be related to the presence of Li_{Mn}-type defects which are not involved in the formation of the regular magnetic structure. From the data for the position occupancy given in Table 2, one can see that this composition is characterized by the presence of maximum quantity of the lithium ions in the manganese positions. Another important thing that should be noted here, is that for each of the three compositions studied, the value of the
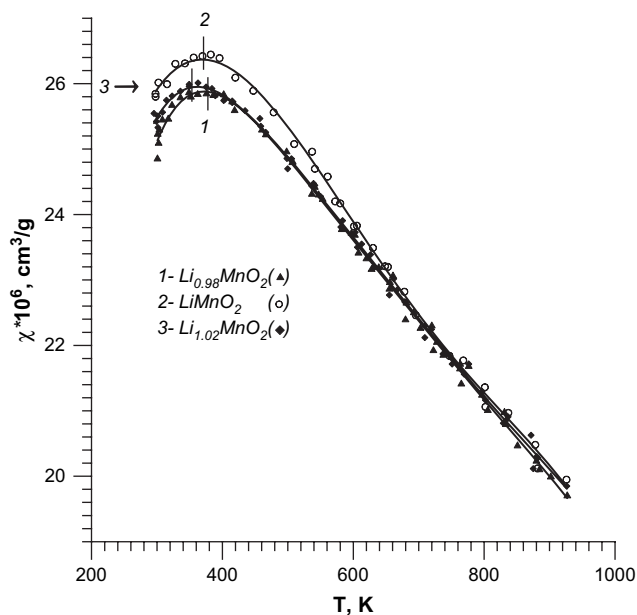

Fig. 5. High temperature part of magnetic susceptibility for Li_xMnO_2. Marks indicate positions of maximum determined by differentiation of experimental data.

Table 5
Refinement parameters for the magnetic structure of Li_xMnO_2 at 1.5 K

		$Li_{0.98}MnO_2$	$Li_{1.00}MnO_2$	$Li_{1.02}MnO_2$
Magnetic cell	a (Å)	5.604(2)	5.608(2)	5.609(2)
	b (Å)	9.065(2)	9.068(1)	9.076(2)
	c (Å)	11.482(6)	11.487(8)	11.490(5)
Mn(2a)	x/a	0.125	0.125	0.125
	y/b	0.125	0.125	0.125
	z/c	0.3165(5)	0.3176(6)	0.3177(9)
	$U_{iso} \times 100$	0.49(5)	0.94(5)	1.70(6)
Magnetic moment of Mn^{3+}	Moment value (μ_B)	3.52(5)	3.56(6)	3.27(2)
	Moment direction	[010]	[010]	[010]
Calculated density (g cm^{-3})		4.216	4.264	4.397
Agreement factors	ωR_p	4.72	6.09	6.12
	R_p	3.74	4.49	4.73
	χ^2	2.438	2.626	4.446
	$R(F^2)$	7.81	5.39	5.61
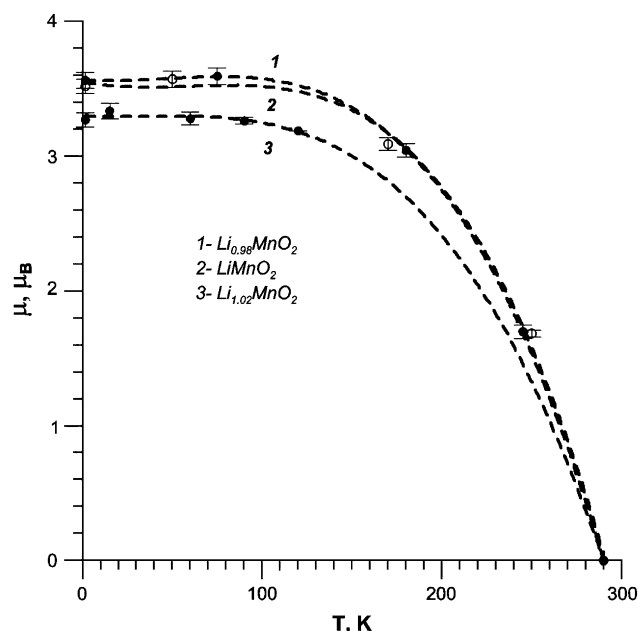
Fig. 6. Temperature dependence of magnetic moments obtained from neutron-diffraction data.
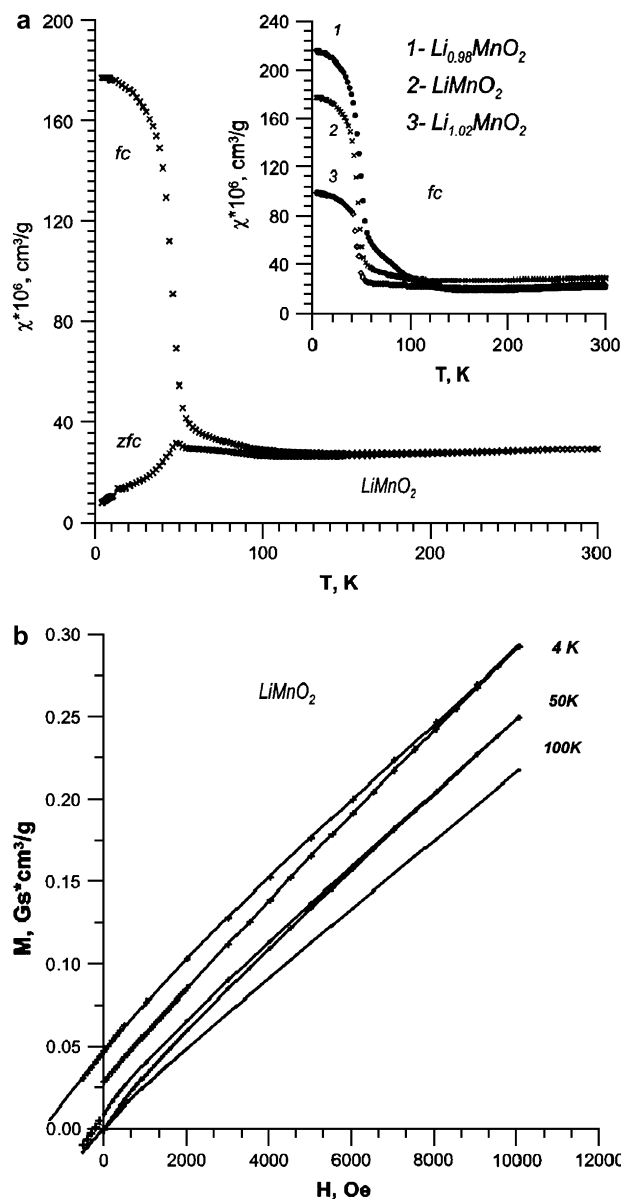

Fig. 7. Magnetic susceptibility data for zero cooled (zfc) and field cooled (fc) samples of lithium manganese oxides; applied field = 100 Oe (a); magnetization of $LiMnO_2$ (b).

magnetic moment is significantly lower than the theoretical value for Mn^{3+} ($3d^4$), i.e. $4\,\mu_B$. Greedan et al. [9] reported the reduced value of the magnetic moment of 3.69(4) μ_B/Mn^{3+} for $LiMnO_2$ too. In our opinion, this fact points to the previously discussed phenomenon of a partial disorder of the structure leading to a reduction of the number of the manganese ions which participate in the formation of the magnetic structure.

The temperature that corresponds to the magnetic order transition is not observed in a $\chi(T)$ curve (Fig. 7a), however, it can be easily determined from temperature dependence, $d(\chi T)/dT$. The basis for this are the conclusions drawn in Ref. [20] where the temperature dependence of the heat capacity for an antiferromagnetic system correlates with the temperature dependence of the derivative of the magnetic susceptibility with respect to the temperature. As followed from a λ-type dependence given in Fig. 8, the temperature of the antiferromagnetic ordering is 259 K (it is close to results of Ref. [9]) and it is independent of the composition. Above this temperature, a long-range 3D magnetic order is distorted but the exchange-bound clusters are still present. For their distortion, a significantly higher energy is required — it can be estimated by the temperature compatible with the maximum of the magnetic susceptibility (Fig. 5).

At the temperatures below 100 K, a discrepancy in fc- and zfc-dependences of the magnetic susceptibility has been observed for each of the Li_xMnO_2 compositions. In agreement with the sharp increase of the susceptibility when the temperature decreases, the discrepancy points out to the appearance of a ferromagnetic component. An example of the low-temperature part of the magnetic susceptibility of stoichiometric $LiMnO_2$ is shown in Fig. 7a.

As was already mentioned above, a weak ferromagnetism (small sublattice canting) can be the reason for the ferromagnetic component in the antiferromagnetic phase. It turns out that the sensitivity of the neutron-diffraction investigations carried out both within this study and by the authors of Ref. [9] was inadequate to determine any direction and value of the magnetic moments. However, both the decrease of the magnetic moment (Fig. 6) determined for the antiferromagnetic structure in the area of the presence of the assumed weak ferromagnetic state (WFM) and the hysteresis of the magnetization in the same temperature region (Fig. 7b) favor the hypothesis considered. Moreover, the fact that the WFM originates at the temperature being considerably lower than the Néel one is a characteristic feature of WFM in both the stoichiometric and defective lithium manganese oxide.
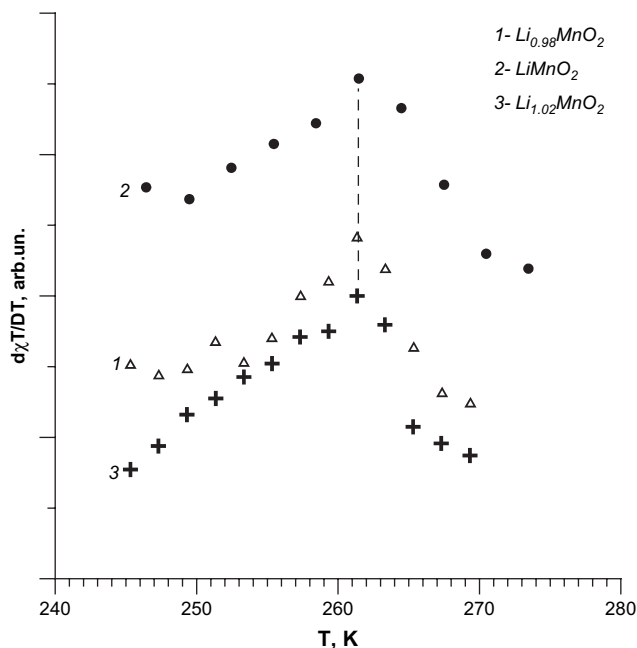
Fig. 8. Temperature dependence of $d\chi(T)/dT$ function for Li_xMnO_2.

Fig. 9. Exchange interactions in Li-deficit $LiMnO_2$.

It is interesting to understand the reason which is responsible for the ferromagnetic component formation at around 50 K in the 3D antiferromagnetic Li_xMnO_2. Our calculations show that Mn_{Li}-type defects, the presence of which is demonstrated by the experimental structural investigations, may play an important role.

3.4. First-principles calculations of the exchange-interaction parameters in $(Li_{15}Mn)Mn_{16}O_{32}$

Using first-principles approach, we also studied a hypothetical structure of $(Li_{15}Mn)Mn_{16}O_{32}$ where the lithium atoms located between the Mn double layers are replaced by manganese atoms (Table 4, Fig. 9). A comparison of the effective exchange-interaction parameters calculated for such "defective" structure with those for $Li_{16}Mn_{16}O_{32}$ mentioned above, allows us to draw the following conclusions: due to a strong exchange interaction between the "defect" (manganese atom in lithium position) and the nearest manganese atom from the double layer ($J_{def} = -49.71$ meV), the interlayer interaction decreases by a factor of 1.6, whereas a weak antiferromagnetic interaction between double layers of manganese changes to ferromagnetic and becomes stronger. Thus, the theoretical results demonstrate that the ferromagnetic component that is predicted from the magnetic measurements given in Fig. 7a (*inset*) may be due to the presence of the manganese ions in lithium layers.

Another peculiarity that should be mentioned here, is that the strong exchange interaction in the layer ($J_1 = -86.28$ meV and $J_2 = -62.41$ meV) decreases slightly for the "defect" structure ($J_1 = -77.03$ meV and $J_2 = -58.26$ meV) so that these interactions are comparable in magnitude to the exchange interactions between this "defect" and the manganese atoms located in the same plane with the defect along c-
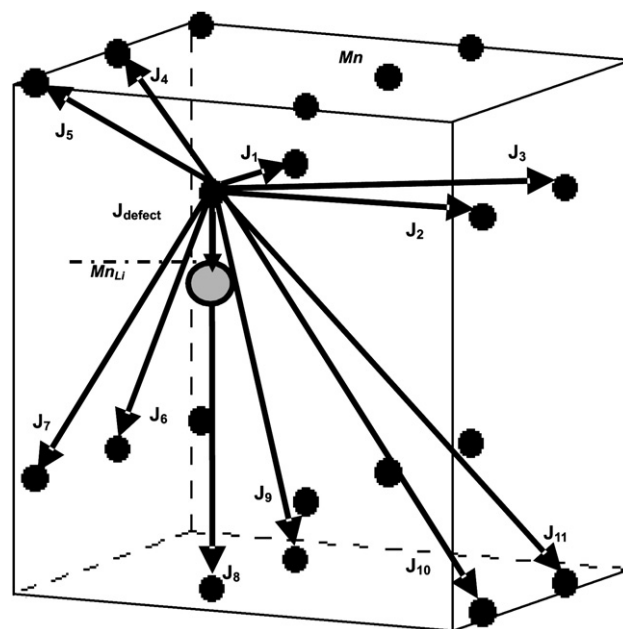
direction, i.e. perpendicular to the Mn layers: namely, the nearest manganese atom ($J_{def} = -49.71$ meV) and the next nearest ones ($J_{1\text{-defect}} = +41.09$ meV and $>J_{9\text{-defect}} = +71.94$ meV). Therefore, we conclude that the presence of the defects make the structure to be isotropic.

4. Summary

The crystal structure of $Li_{0.98}MnO_2$, $Li_{1.00}MnO_2$, and $Li_{1.02}MnO_2$ studied using both neutron and X-ray data is found to be partially disordered due to the presence of manganese ions in lithium positions (Mn_{Li}) and lithium ions in manganese ones (Li_{Mn}). The defects are responsible both for the difference between magnetic properties of Li_xMnO_2 with various Li/Mn ratios and for the appearance of weak ferromagnetism. The latter was demonstrated by the first-principles calculations for the hypothetical $(Li_{15}Mn)Mn_{16}O_{32}$.

The reduction both of the oxygen octahedra distortion in $Li_{0.98}MnO_2$, $Li_{1.00}MnO_2$, and $Li_{1.02}MnO_2$ and Jahn–Teller effect as temperature decreases were observed. Exchange interactions between infinite $Mn^{3+}-\cdots Mn^{3+}-\cdots Mn^{3+}$ chains were considered as the possible reason for this phenomenon.

References

[1] R.J. Gummow, M.M. Thackeray, J. Electrochem. Soc. 141 (1994) 1178.
[2] R.J. Gummow, D.C. Liles, M.M. Thackeray, Mater. Res. Bull. 328 (1999) 1249.
[3] S.-T. Myung, S. Komada, N. Kumagai, J. Electrochem. Soc. 149 (2002) A1349.

[4] F. Le Gras, P. Strobel, M. Anne, D. Bloch, J. Mater. Chem. 7 (1997) 2519.

[5] A.D. Robertson, A.R. Armstrong, A.J. Paterson, M.J. Duncan, P.G. Bruce, J. Mater. Chem. 13 (2003) 2367.

[6] G. Ditrich, R. Hoppe, Z. Anorg. Allg. Chem. 368 (1969) 262.

[7] G. Ceder, S.K. Mishra, Electrochem. Solid State Lett. 2 (1999) 550.

[8] P.F. Bongers, Magnetic properties and chemical bonding, in: Crystal Structure in Inorganic Chemistry, Proceedings of the International Symposium, Wageningen, Netherlands, 1974.

[9] J.E. Greedan, N.P. Raju, I.J. Davidson, J. Solid State Chem. 128 (1997) 209.

[10] D.G. Kellerman, V.S. Gorshkov, V.G. Zubkov, V.A. Perelyaev, V.R. Galakhov, E.Z. Kurmaev, S. Ulenbrock, M. Noimann, Russ. J. Inorg. Chem. 42 (1997) 1012.

[11] E.V. Zaboloztkaya, L.V. Zolotukhina, V.S. Gorshkov, V.V. Karelina, D.G. Kellerman, Russ. J. Inorg. Chem. 46 (2001) 1224.

[12] A.C. Larson, R.B. Von Dreele, "GSAS" LANSCE, MS-H805, Los Alamos Natr. Lab, Los Alamos, NM87545, 1994.

[13] O.K. Andersen, O. Jepsen, M. Sob, Electronic Band Structure and its Applications, in: M. Yussouff (Ed.), Springer-Verlag, Berlin, 1986.

[14] A.I. Lichtenstein, V.I. Anisimov, J. Zaanen, J. Phys. Rev. B 52 (1995) R5467.

[15] L. Croguennec, P. Deniard, R. Brec, A. Lecerf, J. Mater. Chem. 5 (1995) 1919.

[16] J.D. Dunitz, L.E. Orgel, J. Phys. Chem. Solids 3 (1957) 318.

[17] S. Krupichka, Physik der Ferrite und der Magnetiscen Oxide, Academia Verlag, Prague, 1973.

[18] S. Tikadzumi, Physics of Ferromagnetism, Magnetic Characteristics and Practical Use, Mir, Moscow, 1987.

[19] J. Kanamori, J. Prog. Theor. Phys. (Kyoto) 17 (1957) 197.

[20] M.E. Fisher, Proc. R. Soc. (London) A 254 (1960) 66.